

Image registration and super resolution from first principles

Colin B. Clement,¹ Matthew Bierbaum,¹ and James P. Sethna¹

¹*Laboratory of Atomic and Solid State Physics, Cornell University, Ithaca, New York 14853-2501, USA*

(Dated: December 15, 2024)

Image registration is the inference of transformations relating noisy and distorted images. It is fundamental in computer vision, experimental physics, and medical imaging. Many algorithms and analyses exist for inferring shift, rotation, and nonlinear transformations between image coordinates. Even in the simplest case of translation, however, all known algorithms are biased and none have achieved the precision limit of the Cramer Rao bound (CRB). Following Bayesian inference, we prove that the standard method of shifting one image to match another cannot reach the CRB. We show that the bias can be cured and the CRB reached if, instead, we use Super Registration: learning an optimal model for the underlying image and shifting that to match the data. Our theory shows that coarse-graining oversampled images can improve registration precision of the standard method. Finally, while sub-pixel errors in shift inference do not dramatically change the reconstructed image for oversampled data, we show that using our new registration method can lead to $10\times$ more precise particle tracking.

INTRODUCTION

Image registration is the problem of inferring the coordinate transformation between two (or more) noisy and shifted (or distorted) signals or images. This deceptively simple process is fundamental for stereo vision [1], autonomous vehicles [2], gravitational astronomy [3], remote sensing [4, 5], medical imaging [6, 7], microscopy [8], and nondestructive strain measurement [9]. For example, imaging sensitive biological materials [10, 11] and metal organic frameworks [12, 13] with Transmission Electron Microscopy requires combining multiple low-dose high noise images to obtain a viable signal. While most techniques are accurate for very low noise images, errors significantly larger than theoretical bounds can occur for a signal-to-noise ratio as low as 20 (i.e. noise 5% of the signal amplitude); so far general quantification of this error has been elusive.

Much has been written about the uncertainty of shift estimations by analyzing the information theoretic limit known as the Cramer-Rao bound (CRB) [14–16]. These works observed that no known estimators achieve the CRB for image registration. This sub-optimal performance has been blamed on biased estimators: some claim interpolation errors explain the bias [4, 17–19] and others claim that the problem is inherently biased [14]. More works have explored non-perturbative estimations of the uncertainty, which yield larger estimates more consistent with measured error, but which rely on assumptions about the latent image [20–22].

Here we solve these problems, proving no bias in the periodic case, and find that the CRB cannot be reached when transforming one image to match another. Beginning with a statistical model of image formation and Bayesian inference, we derive the canonical and intuitive least-squares objective function by integrating out the unknown image. This analysis requires the inverse transformation of the data, achieved by interpolation which

has already been found culpable of bias in registration. We show that there is no bias for periodic images and predict that the errors grow quadratically with noise (the CRB predicts a linear relationship). Our analysis suggests that bias depends only on the image boundaries. Using our theory, we conclude that coarse-graining raw data (perhaps counter-intuitively) can significantly improve the precision of the standard method.

Ultimately, we determine that one must learn and shift a model of the underlying image in order to most precisely and accurately infer shifts between noisy images. We support this claim first by achieving errors consistent with the CRB with periodic image registration. Following the full Bayesian cycle of model selection, we demonstrate that correct inference of the image shifts depends critically on selecting a model for the underlying image which is supported by the data. Inspired by the inextricable relationship between image registration and super-resolution, we name this new method Super Registration (SR). We show the success of this approach with general non-periodic images, which achieves nearly zero bias and an error which scales linearly with noise. For oversampled data, our reconstructed images do not vary drastically from those produced by the standard method. In spite of this, we demonstrate $10\text{--}20\times$ more precise particle tracking positions when inferred from correctly registered images. We conclude by discussing the consequences of our analysis on more general nonlinear registration [23], and registration of images captured with different imaging modes.

THEORY OF IMAGE FORMATION

In this work, image registration will be restricted to the task of inferring a rigid shift relating two (or more) discretely sampled noisy images with sub-pixel precision. More general transformations are accommodated by our

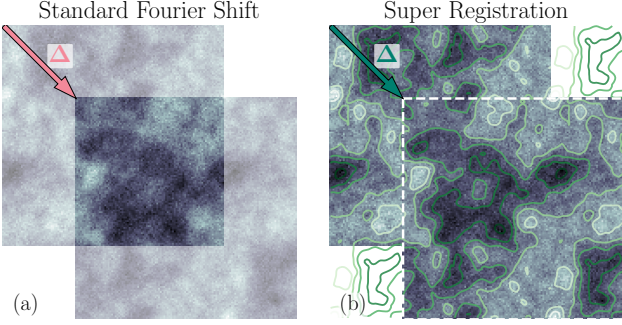


FIG. 1. Illustrations of image registration techniques. (a) A schematic of the standard method of image registration which measures the shift Δ between noisy data (greyscale images) by shifting one to match the other. (b) A schematic of our proposed method, Super Registration, which infers the shift Δ instead by learning the underlying image I (green contours), and shifting the coordinates until the model image best fits the data (greyscale images).

subsequent arguments through application of the chain rule. Defining some true image (called latent, to be discovered) intensity function $I(\mathbf{x})$ with $\mathbf{x} \in \mathbb{R}^2$, we measure at least two images by sampling discretely:

$$\begin{aligned}\phi_i &= I(\mathbf{x}_i) + \xi_i \\ \psi_i &= I(\mathbf{x}_i + \Delta) + \xi_i,\end{aligned}\quad (1)$$

where ϕ_i is the i^{th} pixel of image ϕ and ξ_i are white noise distributed with zero mean and variance σ^2 , and Δ is the shift between the images which we intend to infer.

Equation 1 is our model, which we can more fruitfully express as the likelihood $p(\phi, \psi | \Delta, I)$ of measuring ϕ and ψ given I and Δ :

$$p(\phi, \psi | \Delta, I) \propto \exp \left(\frac{-1}{2\sigma^2} (||\phi - I||^2 + ||\psi - T_\Delta I||^2) \right), \quad (2)$$

where $\|\mathbf{x}\|^2 = \sum_i x_i^2$. T_Δ represents the operator which translates its argument by Δ , for a continuous image $T_\Delta I(\mathbf{x}) = I(\mathbf{x} - \Delta)$. We interpret this distribution as our image model fluctuating around data. Note that Eq. 2 accommodates multi-image registration by multiplying more products of terms comparing images to the shifted latent image I .

In order to infer Δ after measuring the images ϕ and ψ we must reverse the conditional probability in Eq. 2 using Bayes theorem. The posterior (post-measurement) probability $p(\Delta, I | \phi, \psi)$ of Δ and I is

$$p(\Delta, I | \phi, \psi) = \frac{p(\phi, \psi | \Delta, I) p(\Delta, I)}{p(\phi, \psi)}. \quad (3)$$

$p(\Delta, I)$ is called the prior probability and $p(\phi, \psi)$ is called the evidence because, as we later show, it can be interpreted as the probability of our data given our choice of model. The task of inferring Δ is achieved by maximizing this posterior probability. We define the maximum

likelihood estimator of Δ to be

$$\begin{aligned}\Delta^* &= \max_{\Delta, I} p(\Delta, I | \phi, \psi), \\ &= \max_{\Delta, I} p(\phi, \psi | \Delta, I) p(\Delta, I),\end{aligned}\quad (4)$$

where the second line is possible because the evidence is independent of Δ and I .

How accurately should we be able to measure Δ ? If we assume we know the underlying image I , the answer is given by the Cramer-Rao bound (CRB) [24], which is related to the inverse of the Fisher Information matrix (FIM)

$$g_{\mu\nu} = \left\langle \frac{\partial^2 \log p}{\partial \theta_\mu \partial \theta_\nu} \right\rangle, \quad (5)$$

where $p = p(\Delta, I | \phi, \psi)$ is the posterior given by Eq. 3 and θ_μ are the parameters, i.e. Δ and I . For intuition, assuming we know the underlying image I , and that $\partial I / \partial x$ and $\partial I / \partial y$ are uncorrelated, the smallest possible variance on the estimation of Δ_x the x -direction shift is

$$\sigma_{\Delta_x}^2 \geq \sigma^2 \left/ \int d^2 \mathbf{x} \left(\frac{\partial I}{\partial x} \right)^2 \right.. \quad (6)$$

In other words, if the data are very noisy or if the underlying image has no features, it will be difficult to measure the shifts. Note that the CRB predicts that the shift error will scale linearly with noise ($\sigma_\Delta \propto \sigma$). We reiterate that this is the CRB of the shifts assuming knowledge of the true image I . Since this is an unrealistic assumption for real data, we call Eq. 6 and its discrete analog the naïve CRB. For previous derivations and discussions of the naïve CRB for image registration, see [14, 15]. When discussing the CRB below we use the definition related to Eq. 5 and not the intuitive result of Eq. 6.

Deriving the standard method of image registration

In an experiment we have no access to the latent image I . We offer a new derivation of the standard method for overcoming this by marginalizing, or integrating out I :

$$p(\Delta | \phi, \psi) \propto \int dI p(\phi, \psi | \Delta, I) p(I). \quad (7)$$

If we assume all images are equally likely ($p(I) \propto 1$), we can perform the integral by first recognizing that $||\psi - T_\Delta I||^2 = ||T_{-\Delta} \psi - I||^2$ if T_Δ is a unitary transformation (preserves the L2 norm). Transforming discrete data will require interpolation. Linear, quadratic, cubic, bi-cubic, and other local interpolation schemes previously studied for this problem [4, 17–19] are not unitary—neatly explaining some of their observed bias. In this work we will consider only unitary interpolation by using Fourier shifting, however our ultimate solution will obviate this discussion by directly employing Eq. 2. Now

the posterior $p(\Delta|\phi, \psi)$ is a product of integrals of the form

$$\int dx \exp\left(\frac{-1}{2\sigma^2}((x-a)^2 + (x-b)^2)\right) \propto \exp -\frac{(a-b)^2}{4\sigma^2}. \quad (8)$$

Applying this to each pixel in the data we arrive at the marginal likelihood

$$p(\Delta|\phi, \psi) \propto \exp\left(-\frac{1}{4\sigma^2}\|\psi - T_{-\Delta}\phi\|^2\right). \quad (9)$$

We have derived the standard least-squares similarity measure (it is usually written down intuitively), in which one simply shifts one image until it most closely matches the other. This process is illustrated by Fig.1(a), which shows a pair of synthetic data which will serve as I in our numerical studies of periodic registration. It was calculated by sampling a 64×64 image from a power law in Fourier space

$$P(|I(k)|) \sim k^{-1.8} e^{-\frac{1}{2}(\frac{k}{k_c})^2}, \quad (10)$$

damped by a Gaussian with scale $k_c = k_{\text{Nyquist}}/3$ to ensure a smooth cutoff approaching the Nyquist limit, preventing aliasing.

Notice that if T_Δ is not unitary that this objective is different depending on whether you shift one measured image or the other. Note also that in general image registration this inverse transformation may not exist; in such cases this method will fail. The literature features multiple implementations of Eq. 9 using Fourier interpolation by either shifting the data [25] or upsampling by padding in Fourier space and finding the maximum cross-correlation [26]. The latter method can only be as accurate as the factor of upsampling, e.g. quadrupling (in 2D) the number of Fourier modes allows evaluating shifts of half a pixel. While sophisticated extrapolations have been used to overcome the arbitrary choice of how much to upscale, we will exactly shift the data and optimize Eq. 12 directly. So given a 2D Fourier transform operator \mathcal{F} we implement $T_\Delta\phi$ as:

$$T_\Delta\phi = \mathcal{F}^{-1} e^{-i\mathbf{k}\cdot\Delta} \mathcal{F}\phi \quad (11)$$

Another important result of our theory is the $4\sigma^2 = (2\sigma)^2$ in the denominator of Eq. 9: this likelihood function is for data with twice the variance of our original problem, which is consistent with taking the difference of two noisy signals. Some of the reported discrepancy ($\sqrt{2} \sim 40\%$) between the CRB and observed error [14, 15, 27] can be explained by the absence of this factor. Those studying multi-image registration have also neglected this modification of the noise fluctuations in their estimating of shift precision [27]. We have obtained by integrating out the latent image I a distribution which depends only on our data ϕ and ψ and the unknown shift

Δ . We can now define Δ_m^* , the marginal maximum likelihood (ML) solution, which we will subsequently refer to as the standard Fourier shift (FS) method:

$$\Delta_m^* = \max_{\Delta} p(\Delta|\phi, \psi) = \min_{\Delta} \|\psi - T_{-\Delta}\phi\|^2. \quad (12)$$

Previous authors have argued that image registration is fundamentally biased [3, 14, 21]. While bias is certainly plausible for shifts for which two images barely intersect (so that the edges affect fluctuations), we argue and aim to show that no such significant fundamental bias appears for smaller shifts. Surprisingly, we will see that this argument may in fact be true, due instead to a total derivative depending on the structure of the edges of the underlying image. The next section analyzes the statistical properties of the standard FS method of Eq. 12.

STATISTICAL PROPERTIES OF THE STANDARD METHOD

It is well documented in the literature that the errors in shift inference via FS are much larger than the naïve CRB. Figure 2 shows the noise-averaged error (pink dots) of inferring the shifts as measured using the standard Fourier shift method in Eq. 12. The measured error grows quadratically with the Gaussian additive noise σ , dwarfing the naïve CRB (shaded pink region). The follow section will derive a theory (black dotted) to predict this quadratic error growth.

Say we measure the fields ψ_i and ϕ_i , then the log-marginal posterior is (up to a constant) proportional to

$$\mathcal{L} = \frac{1}{2} \sum_i (\psi_i - T_{-\Delta}\phi_i)^2 = \frac{1}{2} \sum_k |\tilde{\psi}_k - e^{ik\Delta} \tilde{\phi}_k|^2, \quad (13)$$

where $\tilde{\phi}_k$ and $\tilde{\psi}_k$ are the Fourier transforms of our data. Our measurements fluctuate around the true latent image I according to

$$\begin{aligned} p(\psi) &\propto \exp\left(-\frac{1}{2\sigma^2}\|\psi - I(x)\|^2\right), \\ p(\phi) &\propto \exp\left(-\frac{1}{2\sigma^2}\|\phi - I(x - \Delta_0)\|^2\right), \end{aligned} \quad (14)$$

where Δ_0 is the latent shift and σ^2 is the variance of the noise. Near the true shift Δ_0 we can expand the marginal likelihood as

$$\mathcal{L}(\Delta) = \mathcal{L}(\Delta_0) + (\Delta - \Delta_0) \frac{\partial \mathcal{L}}{\partial \Delta} + \frac{1}{2} (\Delta - \Delta_0)^2 \frac{\partial^2 \mathcal{L}}{\partial \Delta^2} + \dots, \quad (15)$$

which is approximately minimized by

$$\Delta - \Delta_0 = -\frac{\partial \mathcal{L}}{\partial \Delta} / \frac{\partial^2 \mathcal{L}}{\partial \Delta^2} = -i \frac{\sum_k k \tilde{\psi}_k e^{-ik\Delta_0} \tilde{\phi}_{-k}}{\sum_k k^2 \tilde{\psi}_k e^{-ik\Delta_0} \tilde{\phi}_{-k}}. \quad (16)$$

By averaging Eq. 16 and its square over the noise we can obtain an estimate of the bias and variance of the marginal shift estimator.

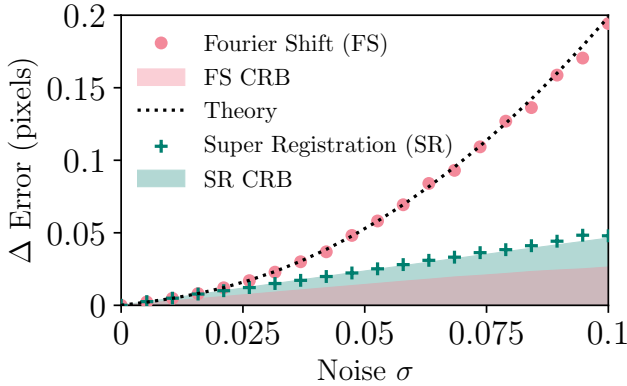


FIG. 2. Comparing the noise-averaged errors of the inferred shift Δ measured by the standard Fourier Shift method and Super Registration in the case of aligning synthetic periodic images. For each data point, we generate an ensemble of 1000 64×64 images according to Eq. 10 and measure the average error for both methods along with the minimum expected error, CRB. We repeat the process for many levels of added noise. The error of the standard method (pink dots) grows quadratically with noise, whereas the naïve CRB (pink shaded region) predicts a linear relationship. Our theory (black dashed line) accurately describes the quadratic dependence in the error, matching numerical experiments. Super Registration (green pluses) demonstrates much lower error, recovers the linear relationship between error and noise, and reaches its CRB (green shaded region). Note that the CRB of Super Registration is larger than the naïve CRB typically used to evaluate the performance of registration methods. It assumes the underlying image is known, and so is an unrealistic bound on the expected error.

Bias of the standard method (1D)

Writing Eq. 16 as A/B we can make progress by Taylor expanding about $A = \langle A \rangle$ and $B = \langle B \rangle$, then averaging over the noise to find

$$\left\langle \frac{A}{B} \right\rangle = \frac{\langle A \rangle}{\langle B \rangle} \left(1 + \frac{\text{var}(B)}{\langle B \rangle^2} \right) - \frac{\text{cov}(A, B)}{\langle B \rangle^2} + \dots, \quad (17)$$

where $\langle \cdot \rangle$ denotes integration over the distributions of Eq. 14. We can obtain a convenient simplification in the case of periodic images by noticing that

$$\langle A \rangle = \left\langle \sum_k k \tilde{\phi}_k e^{-ik\Delta_0} \tilde{\psi}_{-k} \right\rangle = \sum_k k I_k I_{-k}, \quad (18)$$

which is zero because the summand is odd in k . Therefore the average bias for periodic images is to lowest order

$$\left\langle \frac{A}{B} \right\rangle = -\frac{\langle AB \rangle}{\langle B \rangle^2}. \quad (19)$$

In general for non-periodic images $\langle A \rangle \neq 0$. By examining the continuum limit of Eq. 18 in real space we can

gain some insight:

$$\begin{aligned} \langle A \rangle &= \int dx I \frac{\partial I}{\partial x} \\ &= \frac{1}{2} \int dx \frac{\partial}{\partial x} I^2 = \frac{1}{2} (I(x_N)^2 - I(x_0)^2), \end{aligned} \quad (20)$$

where x_N and x_0 are the endpoints of the domain; $\langle A \rangle$ is a total derivative depending only on the edges of the image. We hypothesize that the bias of the standard FS method of image registration shown in Fig. 5 will be dominated by the edges of the data. Ziv and Zakai in 1969 shared this speculation [21], however, whereas they argued that impingement of shift fluctuations onto the limits of the domain caused bias, our theory suggests that structures of the edges of images themselves cause bias.

Evaluating the remaining moments of Eq. 19 we find

$$\langle B \rangle = \sum_k k^2 I_k I_{-k}, \quad (21)$$

which is the roughness of the latent image I in the denominator of the naïve CRB in Eq. 6. The last correlation for the average bias is

$$\langle AB \rangle = \sum_{kk'} kk'^2 e^{-i(k+k')\Delta_0} \langle \tilde{\psi}_k \tilde{\psi}_{k'} \rangle \langle \tilde{\phi}_{-k} \tilde{\phi}_{-k'} \rangle, \quad (22)$$

for which the first and second moments

$$\langle \tilde{\psi}_k \rangle = I_k, \quad \langle \tilde{\phi}_k \rangle = e^{-ik\Delta_0} I_k, \quad (23)$$

$$\langle \tilde{\psi}_k \tilde{\psi}_{k'} \rangle = I_k I_{k'}, \quad \langle \tilde{\phi}_k \tilde{\phi}_{k'} \rangle = e^{-ik2\Delta_0} I_k I_{k'}, \quad (24)$$

$$\langle \tilde{\psi}_k \tilde{\psi}_{-k} \rangle = I_k I_{-k} + \sigma^2, \quad \langle \tilde{\phi}_k \tilde{\phi}_{-k} \rangle = I_k I_{-k} + \sigma^2, \quad (25)$$

will be required. Considering the sum in Eq. 22 in three cases $k' = -k$, $k' = k$ and $k' \neq \pm k$ we can apply the moments to find

$$\begin{aligned} \langle AB \rangle &= \sum_k \left(k^3 ((I_k I_{-k} + \sigma^2)^2 + (I_k I_{-k})^2) + \right. \\ &\quad \left. k \sum_{k' \neq \pm k} k'^2 (I_k I_{-k})^2 \right) = 0, \end{aligned} \quad (26)$$

from which we conclude the entire correlation function vanishes due to each term of the summand being odd in k . Further, numerical evidence and inspection of higher order terms in the expansion of Eq. 17 support the conclusion that for periodic images the standard Fourier shift method of image registration is unbiased.

Variance of the standard method (1D)

Turning our attention to the variance or expected error of the bias given by Eq. 16; an expansion and average of $(A/B)^2$ (simplifying for $\langle A \rangle = 0$) yields to lowest order

$$\text{var} \left(\frac{A}{B} \right) = \frac{\langle A^2 \rangle}{\langle B \rangle^2}. \quad (27)$$

Equation 21 gives us $\langle B \rangle$, so we need only to compute the correlation function $\langle A^2 \rangle$:

$$\begin{aligned} \langle A^2 \rangle &= - \sum_k \sum_{k'} k k' e^{-i(k+k')\Delta_0} \langle \tilde{\psi}_k \tilde{\psi}_{k'} \rangle \langle \tilde{\phi}_{-k} \tilde{\phi}_{-k'} \rangle \\ &= - \sum_k \sum_{k' \neq k} k k' |I_k|^2 |I_{k'}|^2 \xrightarrow{0} 0 \\ &+ \sum_k k^2 ((I_k I_{-k} + \sigma^2)^2 - (I_k I_{-k})^2), \end{aligned} \quad (28)$$

where as before we have decomposed the sum into terms for which $k' \neq k$, $k' = -k$ and $k' = k$. We find that the variance of the bias (which is also the variance of the estimated shifts since we have shown $\langle \Delta \rangle = \Delta_0$) is approximately

$$\sigma_\Delta^2 = \langle (\Delta - \Delta_0)^2 \rangle = 2 \frac{\sigma^2}{D^2} + \frac{L\pi^2}{3} \frac{\sigma^4}{D^4}, \quad (29)$$

where $D^2 = \sum_k k^2 I_k I_{-k}$ is the roughness of the image. We used the fact that $\sum_k k^2 = (2 + L^2)\pi^2/3L \approx L\pi^2/3$ for a one-dimensional signal with L points. The lowest order term in Eq. 29 is twice the naïve CRB shown in Eq. 6, consistent with the fact that the marginal posterior in Eq. 9 has twice the variance of the noise. We have shown that the standard Fourier shift method cannot achieve the naïve CRB. Notice that the variance grows beyond the CRB at a rate proportional to σ^4 and the image size L , so that error grows quadratically with noise. This extra factor of the image volume means that sampling a band-limited (sampled below the Nyquist limit) image at a higher rate—increasing the resolution without increasing information content—can actually decrease the registration precision for the standard Fourier shift method. We discuss and verify this observation following an extension of this theory to two-dimensions.

Variance of the standard method in two dimensions

We now turn to the variance calculation in two dimensions. Generalizing our expansion of the marginal likelihood we find

$$\begin{aligned} \mathcal{L}(\Delta) &= \mathcal{L}(\Delta_0) + (\Delta - \Delta_0)^T \nabla \mathcal{L} \\ &+ \frac{1}{2} (\Delta - \Delta_0)^T \nabla^2 \mathcal{L} (\Delta - \Delta_0) + \dots, \end{aligned} \quad (30)$$

from which we conclude that the two-dimensional analogue of Eq. 16 is

$$\Delta - \Delta_0 = -(\nabla^2 \mathcal{L})^{-1} \nabla \mathcal{L}. \quad (31)$$

If the off-diagonal terms of the Hessian $\nabla^2 \mathcal{L}$ are small compared to the diagonal terms (the image is approximately isotropic), the two dimensions decouple into an

application of Eq. 29 for each dimension. This is generally a good approximation except for contrived data. In this case we find the precision of two-dimensional image registration is approximately

$$\langle (\Delta - \Delta_0)^2 \rangle = \begin{pmatrix} 2 \frac{\sigma^2}{D_x^2} + \frac{N\pi^2}{3} \frac{\sigma^4}{D_x^4} \\ 2 \frac{\sigma^2}{D_y^2} + \frac{N\pi^2}{3} \frac{\sigma^4}{D_y^4} \end{pmatrix}, \quad (32)$$

where N is the number of pixels in the one of the measured images, and $D_x = \sum_k k_x^2 I_k I_{-k}$ and $D_y = \sum_k k_y^2 I_k I_{-k}$ are the horizontal and vertical image roughness. Eq. 32 is used in Fig. 2 (black dotted) where we see excellent agreement with the numerically measured error (pink dots). The excellent agreement—in spite of ignoring the cross terms—can be explained by expanding Eq. 31 for small values of the off-diagonal terms: the lowest order correction averages to zero.

Our analysis has shown that the error of shift estimates of the standard Fourier shift method grow much faster than the CRB. Why do the errors scale quadratically with noise? Mackay found that in general and especially for ill-posed problems (like distinguishing noise from signal), integrating over parameters can yield distributions with stretched and skewed peaks, biasing the maximum and leading to large errors [28]. We integrated over all possible images in order to derive the standard FS registration method. Did this choice sabotage our effort to achieve the ultimate precision? For exponential functions (like a Gaussian or our likelihoods above), there is a deep relationship between optimization and integration through Laplace's method or the method of steepest descent [29]. By integrating over all possible images, we essentially maximized $\log p(\phi, \psi | I, \Delta)$ over I —estimating the latent image—and used that estimate for predicting the shift. This estimate is, however, unreliable as it makes no distinction between the signal and the noise. The high frequency modes of the data, dominated by noise and ironically most discriminating for shift localization, cause the fluctuation of our inferred shifts to be much larger than the CRB. This is illuminated by the following section which considers the process of coarse-graining or binning image data.

Coarse Graining Data can Improve Precision

Our theory for the variance of the shift predicts that $\sigma_\Delta^2 = 2 \frac{\sigma^2}{D^2} \left(1 + \frac{N\pi}{6} \frac{\sigma^2}{D^2} \right)$. The factor of the image volume N in the correction term inspired us to consider reducing N without changing σ or D^2 . Coarse-graining the data by some linear factor a —shown schematically in Fig 3(a)—should not change the CRB assuming the latent image I is smooth on that length scale (or assuming that the data is sampled at least a -times the Nyquist frequency). Assuming that each pixel of the data has noise

of variance σ^2 , the variance of noise for each $a \times a$ block should be $a^2\sigma^2$ (variances of uncorrelated noise add). The denominator of the naïve CRB $D^2 = \sum_k k^2|I_k|^2$ is subtler: the amplitude of each pixel increases by a factor of a^2 ($I_k \rightarrow a^2I_k$), and the block sum only removed Fourier modes with zero amplitude by our assumption above, so $D^2 \rightarrow a^4D^2$. Finally the coarse-grained image will have its coordinates expanded by a , so that the variance should be rescaled by a^2 . Therefore coarsening should modify our variance prediction of the Fourier shift method accordingly:

$$\begin{aligned}\sigma_{\Delta}^2 &= a^2 \cdot 2 \frac{a^2\sigma^2}{a^4D^2} \left(1 + \frac{\pi N/a^2}{6} \frac{a^2\sigma^2}{a^4D^2} \right) \\ &= 2 \frac{\sigma^2}{D^2} \left(1 + \frac{\pi N}{6a^4} \frac{\sigma^2}{D^2} \right).\end{aligned}\quad (33)$$

Our theory predicts that coarse-graining over-sampled images can improve shift inference by reducing the correction term, but that the method can at best yield a variance equal to twice the naïve CRB. Figure 3(b) confirms this relationship, where the black dots indicate the variance of a $N = 1024^2$ image which was oversampled by a factor of 20. Each lighter colored dot series is the variance after coarsening by some factor a , and the solid lines are given by Eq. 33. We see excellent agreement with our theory, and a convergence of the variances onto the $2\sigma^2/D^2$ line. Note that the original image ($a = 1$) variances differ from our theory for large noise: perhaps the limits of large images and large noise are where our approximations in truncating the Taylor expansion in Eq. 27 breaks down.

Note that coarsening smooth images only throws away information which is dominated by noise. When we use the coarsened images in the standard FS method, we implicitly estimate the underlying image but with less noisy modes, and will get a more reliable estimate. In a real experiment without knowledge of the true length scale of the image, we will not know the optimal coarsening length scale. Therefore we propose our generative model which will use Bayesian model selection to infer the image complexity supported by the data.

SUPER REGISTRATION

How can we achieve the ultimate precision for image registration as predicted by the CRB? We have seen that the standard FS method of image registration which directly compares two images has a variance in its shift prediction of the form $\sigma_{\Delta}^2 = 2\sigma_{\text{CRB}}^2(1 + N\pi\sigma_{\text{CRB}}^2/6)$, where the CRB is $\sigma_{\text{CRB}}^2 = \sigma^2/\sum_k k^2 I_k I_{-k}$. We are still studying periodic images, so it is natural to consider removing noise with a filter like the optimal Wiener filter. This manifests by modifying our log-marginal likelihood in Eq. 13 with the rule $\psi_k \rightarrow A_k \psi_k$ and $\tilde{\phi}_k \rightarrow A_k \tilde{\phi}_k$,

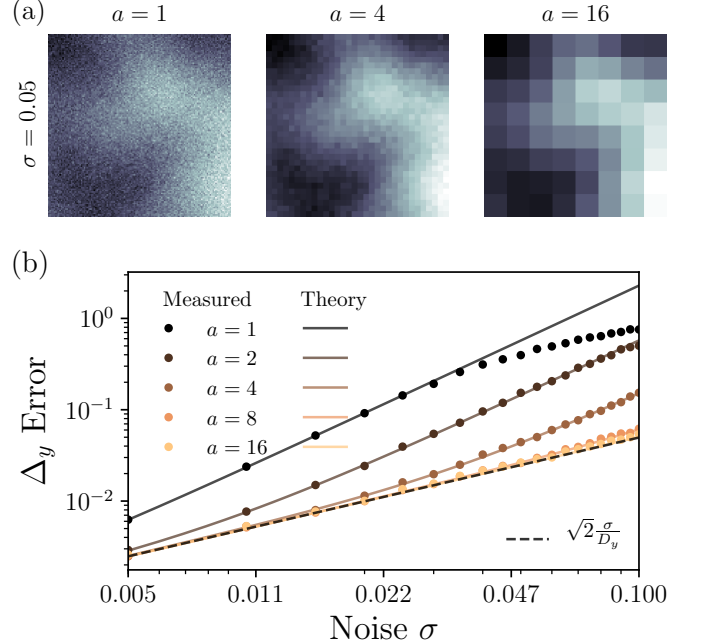


FIG. 3. (a) An oversampled 1024^2 image (the image varies on a scale $20\times$ smaller than the Nyquist frequency limit) with 5% additive white Gaussian noise then coarse-grained by summing over $a \times a$ blocks. Shown are $a = 1$, $a = 4$, and $a = 16$, representing a drastic reduction in image size while not removing any information which localizes the shifts between images. (b) The error in inferred shifts (dots) for the standard Fourier shift method applied to the image after coarsening by 1, 2, 4, 8, and 16 blocks. The original image was chosen to be smooth enough so that coarsening by a factor of 16 would not violate the Nyquist sampling theorem. We see that as we coarsen the image, the error reduces until it reaches $\sqrt{2}$ times the naïve CRB, $\sqrt{2}\sigma/D_y$. The solid lines are the predictions of our theory, which show that coarse-graining reduces the higher order correction to the variance. Coarse-graining the images can improve the precision of the standard Fourier shift method, until it reaches the Nyquist limit, then the loss of information will cause bias.

for some filter function A_k . This modification simply changes $\sigma_{\text{CRB}}^2 \rightarrow \sigma^2/\sum_k k^2 A_k I_k A_{-k} I_{-k}$, and since $A_k A_{-k} \leq 1$ (a filter only reduces power), this can only increase σ_{CRB}^2 and thus reduce our precision.

Faced with this fact we abandon the standard method of image registration and return to first principles by studying the likelihood defined by the image formation model in Eq. 2. Instead of shifting the data, we will model the image and shift that, as shown schematically in Fig. 1. This method will result in a de-noised and, depending on the data, a super-resolution estimate of the latent image. Inspired by the inextricable relationship between registration and super-resolution that we have discovered, we call our new method Super Registration (SR). Our success depends on using all that Bayesian inference has to offer, and so we proceed with a discussion of evidence-based model selection.

Bayesian inference and model selection

Following Mackay's discussion on integration versus optimization in inference with hyperparameters we will choose a model space and from this select the best model by comparing the model evidence, $p(\phi, \psi)$. The evidence is simply the normalization constant of the posterior Eq. 3; its utility for selecting the best model can be exposed by a seemingly erudite increase in notational complexity which makes manifest more of the assumptions in our model. Consider a model of image formation for the case of periodic image registration, expressed as the likelihood of measuring two images $p(\phi, \psi | \Delta, I)$. Now that we are optimizing over I instead of integrating, we must choose some parameterization $I \in \mathcal{H}$ where \mathcal{H} is some space of image models, e.g. a Fourier series or sums of polynomials. This choice must be reflected in the conditionals of our probabilities, so that the likelihood of measuring ϕ and ψ must now be written $p(\phi, \psi | \Delta, I, \mathcal{H}_\lambda)$, where \mathcal{H}_λ represents a specific choice of image model.

Proceeding with the inference task at hand by writing again (with our new notation) the result of Bayes' theorem shown in Eq. 3 we see that the posterior now reads

$$p(\Delta, I | \phi, \psi, \mathcal{H}_\lambda) = \frac{p(\phi, \psi | \Delta, I, \mathcal{H}_\lambda) p(\Delta, I | \mathcal{H}_\lambda)}{p(\phi, \psi | \mathcal{H}_\lambda)}. \quad (34)$$

The solution to our problem still lies in studying this posterior distribution, but we now must also infer the best model \mathcal{H}_λ . We again apply Bayes' theorem, finding the probability that our model is true given our measured images

$$p(\mathcal{H}_\lambda | \phi, \psi) \propto p(\phi, \psi | \mathcal{H}_\lambda) p(\mathcal{H}_\lambda). \quad (35)$$

We have explicitly ignored the normalization constant $p(\phi, \psi)$ [30]. Assuming we have no prior preference for some models over others, $p(\mathcal{H}_\lambda) \sim 1$, so inferring which model is most likely given the data is equivalent to maximizing $p(\phi, \psi | \mathcal{H}_\lambda)$, which is the normalization of Eq. 34.

Therefore Bayesian inference for image registration consists of the following steps given some data ϕ and ψ .

1. Choose some model \mathcal{H}_λ and evaluate the posterior $p(\Delta, I | \phi, \psi, \mathcal{H}_\lambda)$.
2. Summarize the posterior by calculating the position and widths of the maximum likelihood Δ and I .
3. Evaluate the model evidence $p(\phi, \psi | \mathcal{H}_\lambda)$.
4. Repeat steps 1-3 with some subset of the model space \mathcal{H} .
5. Choose the model \mathcal{H}_λ with the largest evidence and examine its concomitant posterior distribution.

The final (unlisted) step is to examine and decide whether the residuals and the maximum likelihood image and shifts are reasonable.

This recursive process of acknowledging all the context and condition of our model and inverting them with Bayes theorem can go on forever. We could for instance consider a probability over the parameters θ of our model $\mathcal{H}_\lambda(\theta)$, adding another integration or optimization to the steps above. Fortunately, the deeper these model assumptions go, the less these decisions affect the outcome of our inference [28]. Bayesian inference does not exclude the experience of the researcher; we will terminate the inference recursion with our own judgement.

Super Registration for periodic images

Returning to our periodic image registration problem, let us pursue the inference steps above in a concrete example. The natural model space for periodic images consists of Fourier series, indexed by the maximum frequency allowed. Given two images ϕ and ψ , the probability of measuring these images given some latent image I and shift Δ is

$$\begin{aligned} \log p(\phi, \psi | \Delta, I, \mathcal{H}_\lambda) = & -\frac{1}{2\sigma^2} \sum_{k=0}^{\lambda} |\phi_k - I_k|^2 + \\ & |\psi_k - e^{-i\mathbf{k} \cdot \Delta} I_k|^2 \\ & - \log Z_L, \end{aligned} \quad (36)$$

where λ indexes the complexity of the model and ϕ_k, ψ_k, I_k are the components of the Fourier transforms of our image model, and Z_L is the normalization. Assuming a constant prior on shifts and images, the maximum likelihood of the shifts and image is the solution of

$$\Delta_{\text{ML}}, I_{\text{ML}} = \min_{\Delta, I} \sum_{k=0}^{\lambda} |\phi_k - I_k|^2 + |\psi_k - e^{-i\mathbf{k} \cdot \Delta} I_k|^2. \quad (37)$$

Equation 37 is in the standard form of a nonlinear least square problem which we solve by alternating linear least squares for I_k and using Levenberg-Marquardt for Δ . For a given image model \mathcal{H}_λ we can find the most likely shift and image by evaluating Eq. 37, calculate the covariance, and compute the evidence. Assuming flat priors on Δ, I_k and \mathcal{H}_λ the evidence is the integral of our likelihood over Δ and I :

$$Z_L = \int dI_k d\Delta p(\phi, \psi | \Delta, I, \mathcal{H}_\lambda). \quad (38)$$

Z_L can be computed by applying Laplace's method of integration using the Jacobian of the least squares problem.

Figure 4 shows the result of step 4 of our algorithm for the periodic data used in all numerical experiments

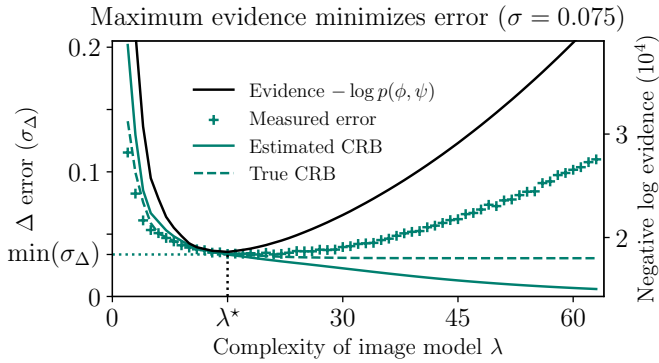


FIG. 4. Using 1000 pairs of 64×64 images generated by Eq. 10 with 7.5% additive Gaussian noise, we computed Eq. 36, the normalization of the posterior probability distribution. As shown in Eq. 35, this quantity can be interpreted as the posterior probability of the model given the data $p(\mathcal{H}_\lambda | \phi, \psi)$, the evidence. We computed this quantity (black curve) for all Fourier cutoffs indexed by λ , showing that when the evidence is maximized the actual shift error (green crosses) is minimized. This error is nearly indistinguishable from the CRB (green dashed). Finally, the naïve estimate of the CRB (solid green) is computed from the curvature of the posterior using Eq 5, the Fisher Information. This estimate continues to decrease with λ as it cannot distinguish signal and noise. During a real experiment only the evidence (black curve) and the naïve curvature estimate of the CRB (solid green) are available, but when the evidence is maximized all estimates of the error match.

so far (shown in Fig. 1), where have used every possible Fourier cutoff. We have inverted the evidence to guide the eye, so that the minimum of the black curve is the most likely model. For this true image and noise level the most likely model is $\lambda = 15$ (15×15 sinusoids). The smallest observed error (green crosses) in shift inference is also precisely at $\lambda = 15$, and is consistent with the CRB (green dashed). The most likely model provides the most precise inference of the shifts. The maximum evidence solution has been interpreted to embody Occam’s Razor that the simplest explanation is most likely [31]. Therefore evidence-based model selection can systematically infer the number of degrees of freedom as supported by the data, avoiding over-fitting and larger errors than the CRB.

The solid green line of Fig. 4 is the CRB estimated by evaluating the second derivative of the log-likelihood; notice that this erroneously continues to decrease with increasing complexity. In a real experiment we only have access to the evidence (solid black line) and this curvature estimate of the CRB (solid green line). The maximum evidence model is also where all of our estimates of the shift error, motivating further the utility of the evidence-based choice of model complexity. Finally note that when the complexity is chosen to be 64 (or all Fourier modes are used) the measured error $\sigma_\Delta \approx 0.1$. In Fig. 1, when the noise is $\sigma = 0.075$, the same as in the evidence ex-

periment above, the observed error of the standard FS method is also $\sigma_\Delta \approx 0.1$. Therefore we see numerical correspondence between integration over the underlying image and optimization without selecting model complexity by considering the evidence.

General non-periodic Super Registration

Following the clarity of studying image registration in the periodic case, we turn our attention to general non-periodic images. Here there is no clearly natural model; images are extremely complicated. While there are exciting candidates in the form of deep convolutional neural networks, these objects cannot (currently) be evaluating at arbitrary points in space; they have no notion of continuous locality [32]. In general the researcher’s knowledge about the physical objects being imaged should inspire the model space. A very specific and successful example is the Parameter Extraction by Modeling Images (PERI), which modeled almost every aspect of a confocal microscope, extracting enough information from a light microscope to infer the parameters of the van der Waals interaction [33]. Lacking such specific inspiration therefore we chose sums of Chebyshev polynomials, in part because of their excellent approximation properties [34].

We generated non-periodic data from the same distribution in Eq. 10, sampled twice as large (128×128), shifted one by Δ_0 , cropped out a 64×64 region, and added noise. Figure 5 show results for the error (pink dots and green crosses) and bias (pink and green lines) using these synthetic data, as a function of both noise σ (Fig. 5(a)) and true shift Δ_0 (Fig. 5(b)). Pink denotes the standard FS method and green denotes Super Registration. Figure 5(a) shows that the standard FS method has an oscillating bias which is zero at whole and half-pixels, and has an oscillating error which is largest at whole pixel shifts and smallest at half pixel shifts. The pink shaded region is the CRB of the FS method. Figure 5(b) shows super-linear error (pink) growth for FS, compared with our theory from Eq. 32 (black dotted), and a bias (pink line) deviating slowly but consistently from zero.

Figure 5(a) shows that Super Registration has nearly a constant bias (green line) and error (green crosses) as a function of true shift Δ_0 , and bias smaller its CRB (green shaded). The error is much smaller than the standard FS method, and is one-third the error of the FS method when $\sigma = 0.1$ (10% noise). Finally we see in Fig. 5(b) that the error of SR grows linearly with noise. While SR here does not reach the CRB, it scales the same as the CRB. A better image model should result in errors more consistent with the CRB. Because we generated data by randomly sampling in Fourier space, shifting, then cropping, our Chebyshev polynomials cannot perfectly represent that signal. This is an important reminder that

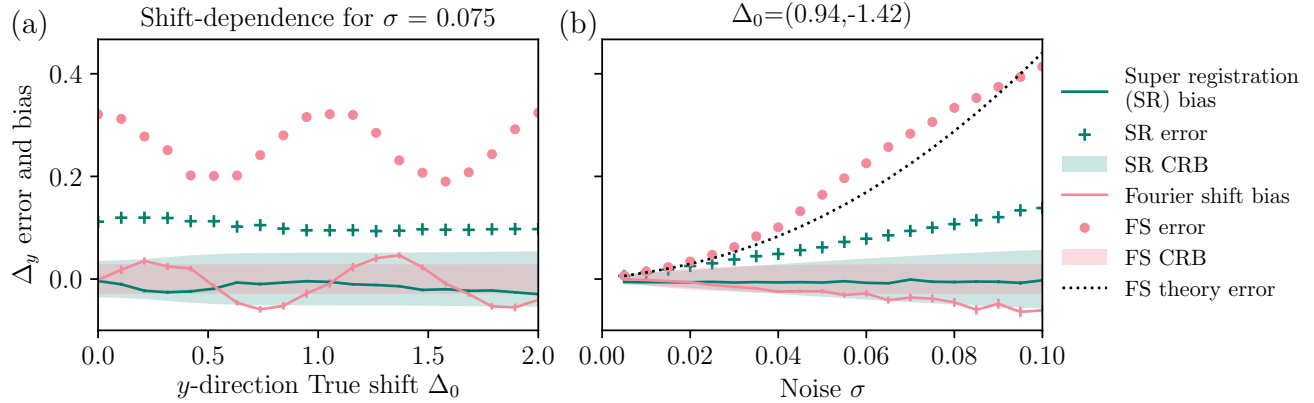


FIG. 5. Comparing the error and bias of the standard Fourier shift (FS) method and Super Registration (SR) for non-periodic data. The synthetic data were generated by Eq. 10 at a higher resolution, Fourier shifted, and then cropped to produce non-periodic images. Errors and biases were measured from 1500 64×64 noise samples. (a) The Δ_y biases, errors, and CRBs for the standard FS (pink) and SR (green) are shown as a function of the true real shift Δ_0 . The standard method suffers from errors (pink dots) and bias (pink line) that are periodic in Δ_0 , with no bias at integer shifts and smallest error at half integer shifts. Super Registration shows almost zero bias (green line) and no periodic structure in the error (green crosses). Similarly to the periodic case, SR is much closer to its CRB (green shaded) than the standard FS method is to its CRB (pink shaded). (b) The biases, errors and CRBs for FS and SR methods as a function of noise for a fixed random shift $\Delta_0 = (0.94, -1.42)$. The standard FS method has super-linear error (pink dots) growth with noise, and a monotonic bias (pink line) large than its CRB (pink shaded). Super Registration has linear error (green cross) growth about twice its CRB (green shaded), and a bias (green line) consistent with zero. SR does not achieve its CRB for this case like it did for the periodic case because the image model is incomplete: we fit images generated from a truncated Fourier series with Chebyshev polynomials.

the CRB depends on the chosen model. Finally we remark on the CRB itself: since the CRB is defined as the inverse of the Fisher Information in Eq. 5, the CRB is model-dependent, and thus the standard FS method and SR have different bounds.

For many experimental images, Super Registration offers only a marginal improvement in the image quality as measured by eye. For a small shift error $\Delta - \Delta_0$ the image intensity reconstruction error is $\Delta I \approx (\Delta - \Delta_0) \cdot \vec{V} I$. For smooth, highly sampled images visual changes will be small. Most experiments do not operate in the regime where they are not sampling at a high enough rate to see the structure of their sample. Although the reconstructions for many experiments will not vary dramatically visually, we now show that the shift errors can dramatically interfere with the information extracted from the reconstructions.

PARTICLE TRACKING ERRORS

A very common task in image processing is tracking particle positions. High precision, especially in atomic-scale TEM and STEM, is important for understanding real-space structure. For example, charge density waves cause atoms to deviate from their lattice by tiny amounts, and can be studied by carefully measuring the positions of the atoms in real space [35]. For High-angle Annular Dark Field (HAADF) STEM, the image of an atom is well-approximated by a 2D Gaussian [23]. Therefore

we created synthetic data of a pair of Gaussian particles, shown in Fig. 6(a) with 10% additive Gaussian noise. Simulating drift in a realistic STEM experiment, we created 8 copies of the two particle images, randomly shifted. For each noise level we sampled 1000 noise instances, with each reconstructing the underlying image with both FS and our Chebyshev-polynomial based Super Registration.

Figure 6(b) shows the error of inferring the position of the larger particle using both the FS reconstruction (pink line) and SR reconstructions (green line). For $\sigma = 0.3$ or 30% noise we see that the precisions of particle position are 10x better using SR than FS. Further, the SR method, not even using the correct model (a sum of Gaussian particles), is only about twice the CRB for particle position inference (black dotted). Finally, when inferring shifts at the optimal coarsening ($a = 3$), we see roughly twice the precision of the standard FS method. In summary we see that even though small shift errors do not have a dramatic effect on the reconstructed image as measured by eye, there are drastic effects on the precision of information extracted from the reconstructions.

CONCLUSION

Through a statistical theory of image formation, we have derived the standard method of image registration, which shifts one image to match another. Our theory predicts that shift errors for the standard FS method grow

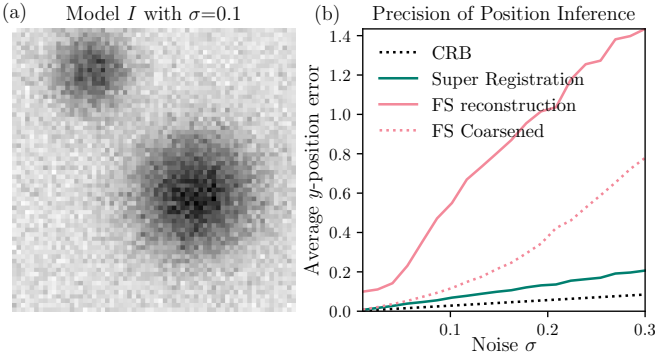


FIG. 6. (a) A model image of two Gaussian particles with 10% Gaussian additive noise. Eight of these images with random sub-pixel relative shifts were generated, and 1000 noise samples were drawn. For each noise sample, the underlying image was reconstructed either by the standard Fourier shift (FS) reconstruction or with Super Registration. With each reconstruction we fit the Gaussian models which generated the data, inferring the most likely particle position and width. (b) The average error of inferring the y -position of the larger particle from images reconstructed with the standard FS method (pink line), a coarse-grained image (pink dotted), and Super Registration (green line). Coarse-graining by a factor of $a = 3$ in this case does not introduce bias and improves particle position inference by a factor of 2. SR improves the particle position inference by a total factor of 10 over the standard FS method, reaching about $2\times$ the CRB for particle position inference. Despite using a general Chebyshev model for the image, we still nearly achieved the CRB in position inference. Using the Gaussian particle model as the model for the underlying image in SR would likely achieve the CRB.

quadratically with noise, much faster than the linear relationship of the CRB. Our explanation for the deviation between the naïve CRB and the standard method comes from a deep relationship between integration and optimization. The resulting formula is useful for designing experiments which require image registration and must be performed using the standard method. Our analysis leads to the surprising fact that coarse-graining the data can improve the shift errors.

We develop a new method of image registration, which models the underlying image, shifts that to match the data, and follows Bayesian inference to select the image model for which there is the most evidence. Our theory reveals an inextricable relationship between image registration and super-resolution—that ultimate shift precision is predicated on selecting a probable model. Therefore we named our new method Super Registration. We showed for periodic images that a Fourier series image model achieves errors consistent with the CRB. We demonstrated superior bias and expected error performance for general non-periodic images, and discussed the shortcomings of our general model. Finally, we showed that, despite marginal improvements in image quality as measured by eye, particle tracking experiments can be

10 \times more precise when using Super Registration reconstructions.

Our results can be extended to more general transformations: by application of the chain rule each term in our calculation of the average bias and variance will be modified by partial derivatives. It is reasonable to assume that the same problems—nonzero bias and errors which are much larger than the CRB—will persist for transformations like affine skews, rotations, and non-rigid registrations. Super Registration can accommodate all of these problems by constructing the forward transformation instead of reconstructing the inverse transformation.

Finally, medical imaging consists of lining up images of the same tissue from different modes like X-ray and Magnetic Resonance Imaging (MRI) [6, 7]. The Super Registration method involves constructing a generative model for the data, and this perspective reminds us that contrast and features in X-ray and MRI will be different because they respond to different underlying tissue structures. Bias and large errors for this problem have been observed and attributed to this fact [36]. Therefore some underlying model of tissue component densities and a model of image formation (Super Registration) will be critical for accurately and precisely registering these images.

Image registration is a very important and fundamental problem in medical imaging, remote sensing, self-driving automobiles, non-destructive stress measurement, microscopy, and more. Our theoretical study of the fundamental problem of rigid shift registration in the presence of noise answers long-standing questions on the precision and accuracy of shift inference, elucidates an inextricable link between registration and super-resolution, and inspires a solution to these problems with wide applicability.

ACKNOWLEDGEMENTS

Thanks to Ismail El Baggari, S.B. Kachuck, K.P. O’Keefe and D.B. Liarte for useful conversations in the preparation of this manuscript. This work was supported by the NSF Center for Bright Beams, award #1549132.

-
- [1] Bruce D Lucas, Takeo Kanade, et al. An iterative image registration technique with an application to stereo vision. 1981.
 - [2] Ryan W Wolcott and Ryan M Eustice. Visual localization within lidar maps for automated urban driving. In *Intelligent Robots and Systems (IROS 2014), 2014 IEEE/RSJ International Conference on*, pages 176–183. IEEE, 2014.
 - [3] David Nicholson and Alberto Vecchio. Bayesian bounds on parameter estimation accuracy for compact coalescing

- binary gravitational wave signals. *Physical Review D*, 57(8):4588, 1998.
- [4] Jordi Inglada, Vincent Muron, Damien Pichard, and Thomas Feuvrier. Analysis of artifacts in subpixel remote sensing image registration. *IEEE transactions on Geoscience and Remote Sensing*, 45(1):254–264, 2007.
- [5] Misganu Debella-Gilo and Andreas Kääb. Sub-pixel precision image matching for measuring surface displacements on mass movements using normalized cross-correlation. *Remote Sensing of Environment*, 115(1):130–142, 2011.
- [6] Lilla Zöllei, John W Fisher III, and William M Wells III. A unified statistical and information theoretic framework for multi-modal image registration. In *IPMI*, pages 366–377. Springer, 2003.
- [7] Michael E Leventon and W Eric L Grimson. Multi-modal volume registration using joint intensity distributions. In *International Conference on Medical Image Computing and Computer-Assisted Intervention*, pages 1057–1066. Springer, 1998.
- [8] Benjamin H. Savitzky, Ismail El Baggari, Colin B. Clement, Emily Waite, Berit H. Goodge, David J. Baek, John P. Sheckelton, Christopher Pasco, Hari Nair, Nathaniel J. Schreiber, Jason Hoffman, Alemayehu S. Admasu, Jaewook Kim, Sang-Wook Cheong, Anand Bhattacharya, Darrell G. Schлом, Tyrel M. McQueen, Robert Hovden, and Lena F. Kourkoutis. Image registration of low signal-to-noise cryo-stem data. *Ultramicroscopy*, 191:56 – 65, 2018.
- [9] Adam D Kammers and Samantha Daly. Digital image correlation under scanning electron microscopy: methodology and validation. *Experimental Mechanics*, 53(9):1743–1761, 2013.
- [10] Alberto Bartesaghi, Alan Merk, Soojay Banerjee, Doreen Matthies, Xiongwu Wu, Jacqueline LS Milne, and Sriram Subramaniam. 2.2 Å resolution cryo-em structure of β -galactosidase in complex with a cell-permeant inhibitor. *Science*, 348(6239):1147–1151, 2015.
- [11] Alberto Bartesaghi, Doreen Matthies, Soojay Banerjee, Alan Merk, and Sriram Subramaniam. Structure of β -galactosidase at 3.2-Å resolution obtained by cryo-electron microscopy. *Proceedings of the National Academy of Sciences*, 111(32):11709–11714, 2014.
- [12] Daliang Zhang, Yihan Zhu, Lingmei Liu, Xiangrong Ying, Chia-En Hsiung, Rachid Sougrat, Kun Li, and Yu Han. Atomic-resolution transmission electron microscopy of electron beam-sensitive crystalline materials. *Science*, 359(6376):675–679, 2018.
- [13] Yihan Zhu, Jim Ciston, Bin Zheng, Xiaohe Miao, Cory Czarnik, Yichang Pan, Rachid Sougrat, Zhiping Lai, Chia-En Hsiung, Kexin Yao, et al. Unravelling surface and interfacial structures of a metal-organic framework by transmission electron microscopy. *Nature materials*, 16(5):532, 2017.
- [14] Dirk Robinson and Peyman Milanfar. Fundamental performance limits in image registration. *IEEE Transactions on Image Processing*, 13(9):1185–1199, 2004.
- [15] Imam Samil Yetik and Arye Nehorai. Performance bounds on image registration. *IEEE Transactions on Signal Processing*, 54(5):1737–1749, 2006.
- [16] Tuan Q Pham, Marijn Bezuijen, Lucas J Van Vliet, CL Luengo Hendriks, and K Schutte. Performance of optimal registration estimators. *Proceedings of SPIE*, 2005 vol. 5817, 2005.
- [17] Gustavo K Rohde, Akram Aldroubi, and Dennis M Healy. Interpolation artifacts in sub-pixel image registration. *IEEE transactions on image processing*, 18(2):333–345, 2009.
- [18] Hubert W Schreier, Joachim R Braasch, and Michael A Sutton. Systematic errors in digital image correlation caused by intensity interpolation. *Optical engineering*, 39(11):2915–2922, 2000.
- [19] Donald G Bailey, Andrew Gilman, and Roger Browne. Bias characteristics of bilinear interpolation based registration. In *TENCON 2005 2005 IEEE Region 10*, pages 1–6. IEEE, 2005.
- [20] Mikhail L Uss, Benoit Vozel, Vitaliy A Dushepa, Vladimir A Komjak, and Kacem Chehdi. A precise lower bound on image subpixel registration accuracy. *IEEE Transactions on Geoscience and Remote Sensing*, 52(6):3333–3345, 2014.
- [21] Jacob Ziv and Moshe Zakai. Some lower bounds on signal parameter estimation. *IEEE transactions on Information Theory*, 15(3):386–391, 1969.
- [22] Min Xu, Hao Chen, and Pramod K Varshney. Ziv–zakai bounds on image registration. *IEEE Transactions on Signal Processing*, 57(5):1745–1755, 2009.
- [23] Andrew B Yankovich, Benjamin Berkels, Wolfgang Dahmen, Peter Binev, Sergio I Sanchez, Steven A Bradley, Ao Li, Izabela Szlufarska, and Paul M Voyles. Picometre-precision analysis of scanning transmission electron microscopy images of platinum nanocatalysts. *Nature communications*, 5:4155, 2014.
- [24] Thomas M Cover and Joy A Thomas. *Elements of information theory*. John Wiley & Sons, 2012.
- [25] Giovanni Jacovitti and Gaetano Scarano. Discrete time techniques for time delay estimation. *IEEE Transactions on signal processing*, 41(2):525–533, 1993.
- [26] Manuel Guizar-Sicairos, Samuel T Thurman, and James R Fienup. Efficient subpixel image registration algorithms. *Optics letters*, 33(2):156–158, 2008.
- [27] Cecilia Aguerrebere, Mauricio Delbracio, Alberto Bartesaghi, and Guillermo Sapiro. Fundamental limits in multi-image alignment. *IEEE Transactions on Signal Processing*, 64(21):5707–5722, 2016.
- [28] David JC MacKay. Hyperparameters: Optimize, or integrate out? In *Maximum entropy and bayesian methods*, pages 43–59. Springer, 1996.
- [29] Nicolaas Govert De Bruijn. *Asymptotic methods in analysis*, volume 4. Courier Corporation, 1970.
- [30] $p(\phi, \psi) = \sum_i p(\phi, \psi | \mathcal{H}_i) p(\mathcal{H}_i)$. This constant changes when we consider more models, which naturally must happen when we obtain more data, but does not influence the preference of one model over another.
- [31] Vijay Balasubramanian. Statistical inference, occam’s razor, and statistical mechanics on the space of probability distributions. *Neural computation*, 9(2):349–368, 1997.
- [32] Dmitry Ulyanov, Andrea Vedaldi, and Victor Lempitsky. Deep image prior. *arXiv preprint arXiv:1711.10925*, 2017.
- [33] Matthew Bierbaum, Brian D Leahy, Alexander A Alemi, Itai Cohen, and James P Sethna. Light microscopy at maximal precision. *Physical Review X*, 7(4):041007, 2017.
- [34] William H Press, Saul A Teukolsky, William T Vetterling, and Brian P Flannery. *Numerical recipes 3rd edition: The art of scientific computing*. Cambridge university press, 2007.

- [35] Ismail El Baggari, Benjamin H Savitzky, Alemayehu S Admasu, Jaewook Kim, Sang-Wook Cheong, Robert Hovden, and Lena F Kourkoutis. Nature and evolution of incommensurate charge order in manganites visualized with cryogenic scanning transmission electron microscopy. *Proceedings of the National Academy of Sciences*, 115(7):1445–1450, 2018.
- [36] David W. Tyler. Intrinsic bias in fisher information calculations for multi-mode image registration. *Opt. Lett.*, 43(10):2292–2295, May 2018.